

Investigation of Physicochemical Drivers Directing Ionic Liquid Assembly on Polymeric Nanoparticles

Sara X. Edgecomb^{1,†}, Christine M. Hamadani^{1,†}, Angela Roberts¹, George Taylor¹, Anya Merrell¹, Ember Suh¹, Davita Watkins², Eden E. L. Tanner^{1*}

¹Department of Chemistry and Biochemistry, The University of Mississippi, University, MS 38677, United States

²Department of Chemical and Biomolecular Engineering, The Ohio State University, Cleveland Ohio, United States

† These authors contributed equally.

*Address for correspondence:

Dr. Eden E. L. Tanner
Department of Chemistry and Biochemistry
The University of Mississippi
University, MS 38677, United States
E-mail: eetanner@olemiss.edu
Phone: 662-915-1165

For submission to Electrochemical Science Advances

Abstract

Ionic liquids (ILs) have emerged as promising biomaterials for enhancing drug delivery by functionalizing polymer nanoparticles (NPs). Despite the biocompatibility and biofunctionalization they confer upon the NPs, little is understood regarding the degree that non-covalent interactions, particularly hydrogen-bonding and electrostatic interactions, govern IL-NP supramolecular assembly. Herein, we use salt (0-1 M sodium sulfate) and acid (0.25 M hydrochloric acid at pH 4.8) titrations to disrupt IL-functionalized nanoassembly for four different polymeric platforms during synthesis. We demonstrate, through quantitative ^1H NMR spectroscopy and Dynamic Light Scattering (DLS), that the driving force of choline trans-2-hexenoate (CA2HA 1: 1) IL assembly varies, and either hydrogen bonding or electrostatics dominate depending on the structure of the polymeric platform. In particular, covalently-bound or branched 50: 50 block copolymer systems (diblock PEG-PLGA (DPP) and Polycaprolactone (PCL)-Polyamidoamine (PAMAM)-based linear-dendritic block co-polymer (LDBC)) are predominantly affected by hydrogen-bonding disruption. In contrast, while a purely linear block co-polymer system (carboxylic acid-terminated poly (lactic-co-glycolic acid (PLGA)) necessitates both electrostatics and hydrogen-bonding to assemble with IL, a two-component electrostatically bound system (electrostatic PEG-PLGA (EPP)) favors hydrogen-bonding with electrostatics serving a secondary role as a driving force.

Introduction

The integration of biocompatible ionic liquids (ILs) in polymeric nanoparticle systems broadly enhance their biomedical applications¹, not only improving the delivery of sparingly soluble drugs² and in antimicrobial applications³, but also allowing new bio-membrane interactions to better facilitate intravenous drug delivery⁴. Ionic liquids (ILs) are low-melting salts ($< 100\text{ }^\circ\text{C}$) consisting of bulky asymmetric cations and anions⁵. Due to the vast structure-to-function physicochemical tunability that is possible⁶⁻⁸, their cationic and anionic components can be engineered to self-assemble onto interfaces through electrostatic interactions and hydrogen bonding⁹⁻¹². This coating then confers protective properties, such as protein-repulsion and cellular biocompatibility, for enhanced circulation half-life¹³. However, at present, there is little understanding regarding the key molecular mechanisms and physicochemical forces driving ionic liquid-polymer nano-assembly.

One of the key determinants that underly the physical chemistry driving IL-nanoparticle surface and bulk reorganization is the structure and chemistry comprising the polymer. This not only defines the polymer's potential for tunability, encapsulation efficiency, and biocompatibility, but also affects its nanoassembly based on hydrophobicity, electrostatics, sterics, and hydrogen

bonding¹⁴. Essentially, these forces play a role in a polymer's critical aggregation concentration (CAC), the point at which small aggregates are formed¹⁵. The degree to which each of these forces are involved in the nanoassembly thus affects the type and range of physicochemical properties between the polymeric nanoparticle (NP) platforms, such as its surface-binding potential and biophysical interactions.

Poly(lactic-co-glycolic acid) (PLGA), an FDA approved polymer for human therapy¹⁶ is the most commonly used polymer-based material for biomedical applications. Because of its high degree of biodegradability, it has been studied for the encapsulation of paclitaxel¹⁷, cancer cell targeting¹⁸, and as a potential protein nanocarrier¹⁹. The PLGA used in this study is a 50: 50 (glycolic acid: lactic acid) linear block copolymer with a carboxylic acid terminal group. The hydrophobic lactic acid influences the formation of small diameter sized (< 200 nm) spherical nanoparticles through the hydrophobic effect. In an aqueous environment, the lactic acid forms a globular center with the polar glycolic acid facing toward the water molecules. The glycolic acid chains offer protection for the hydrophobic chains from the hydrophilic environment, providing a stable core for the encapsulation of hydrophobic molecules for drug delivery applications. Once delivered into the body, the polymer is broken down through hydrolysis of the ester links between the lactic acid and glycolic acid and carried through the tricarboxylic acid cycle to be flushed out of the body as water and carbon dioxide^{20,21}.

In addition to the PLGA, polyethylene glycol (PEG), another FDA approved polymer, can be added for protection against adhesion of undesirable proteins in the blood stream, increasing the half-life of the NPs²². Two ways PEG can be incorporated is by coating the PLGA NPs through adhering to the glycolic acid surface through electrostatic interactions, or engineering a covalent bond to PLGA, forming a diblock copolymer. The difference between the electrostatically bound PEG PLGA (EPP) NPs and the amphiphilic diblock copolymer PEG-b-PLGA (DPP) NPs are the way in which the NPs assemble. The EPP NPs act similarly to the PLGA NPs with the globular hydrophobic center, but instead of the glycolic acid facing the water, the hydrophilic PEG makes a layer on top of the glycolic acid. Hereafter the PEG interacts with the aqueous environment, adding an extra layer of protection for the hydrophobic lactic acid and stability of PLGA NPs in water²³. The DPP NPs form based on the hydrophilic fraction of the diblock copolymer. Anything between approximately 25 and 40% will form nanoparticles called polymersomes²². With the diblock copolymer used in this study, the molecular weight ratio (PEG: PLGA) is 5 kDa to 25 kDa with a hydrophilic fraction of 20%. Polymersomes, unlike PLGA NPs, are vesicles with a wide range of diameter sizes that have a hollow hydrophilic core and a thin hydrophilic outer layer formed from the more hydrophilic PEG. Between the two hydrophilic layers is the hydrophobic PLGA layer, establishing a tri-layer structurally similar to a lipid bilayer or liposomes. Unlike the PLGA NPs, the hydrophilic core provides polymersomes with the advantage of encapsulating big and small hydrophilic and hydrophobic molecules²⁴.

Like the EPP NPs, the linear-dendritic block copolymers (LDBC) are amphiphilic with this study's particular material having polycaprolactone (PCL) as the hydrophobic linear segment and polyamidoamine (PAMAM) as the dendritic (symmetrically branched) hydrophilic segment. However, with its dendritic property, it is a lot bulkier than the traditional linear polymers previously discussed, and these branch points adds another complexity to diblock copolymers. For instance, it changes the physical properties such as viscosity and crystallinity²⁵. The branched and linear portion can be modified synthetically during structure formation to control the size, surface charge, and shape, enabling multifunctional surface properties and high tunability. Despite the difference in structure, LDBC NPs are formed through the same hydrophobic effect with PAMAM ending up as the surface interacting with its aqueous environment. LDBC have also been shown to be effective in loading and delivering hydrophilic and hydrophobic drugs¹³.

Herein, we disrupt electrostatic and hydrogen-bonding forces to elucidate the physicochemical drivers of IL-NP assembly across either functionalized linear block-copolymer (COOH-terminated PLGA or electrostatic PEG-PLGA (EPP)), diblock PEG-PLGA (DPP), or linear-dendritic block copolymer (LDBC) platforms. Electrostatic disruption was performed by titrating 0 -1.0 M Na₂SO₄ into the aqueous phase during synthesis followed by titration to pH 4.8 (below the pK_a of choline trans-2-hexenoate (CA2HA 1: 1) at 5.13) via 0.25 M HCl after synthesis of NPs and during coating with IL to disrupt hydrogen bonding.

Results and Discussion

For each of the four polymeric NP systems, hydrogen bonding and electrostatics directed bare or IL-coated nanoparticle assembly appears to be governed by not only physicochemical interactions with the environment, but also through supramolecular interactions within the polymers. The ionic liquid choline trans-2-hexenoate (CA2HA 1: 1) drives the formation of charged cationic and anionic layers upon the carboxylic-acid terminated on linear PLGA NPs, validated by ¹H-NMR spectroscopy and an increase in hydrodynamic diameter after coating with respective anionic shift in surface charge by Dynamic Light Scattering (DLS). This phenomenon is also observed with PLGA NPs when polyethylene glycol (PEG) (DPP NPs) is electrostatically pre-adsorbed onto the PLGA's carboxylic acid terminated surface. In contrast, covalently bound diblock PEG-PLGA (DPP) NPs differ not only in the environment-surface sterics of the arranged amphiphilic nanoparticle, but also in the forces driving formation of the hydrophobic chains, affecting the range of electrostatic versus hydrogen-bonding interactions when CA2HA 1: 1 is combined with the NPs²⁶. Alternatively, covalently bound Polycaprolactone (PCL)-Polyamidoamine (PAMAM)-based LDBC NPs are formed by first directly solvating polymer in IL^{27,28}, causing hydrogen bonding to direct the majority of the grafted NP bulk while the outermost interfaces are affected by electrostatics. However, it is still yet not well understood the degree to which these interactions play on a molecular-level mechanistic assembly of the ionic liquid

coating. Comparing the titrated polymeric nanoparticles to the native bare and IL-NPs will give insight to the role of these interactions in each NP system.

We begin by considering the PLGA system. In Figure 1A, ^1H NMR spectroscopy reveals that salt treatment on its own causes a partial decrease in anionic components (seen by tracking the signature terminal CH_3 peak at 0.9 ppm) which remains consistent between 0.5 M or 1.0 M Na_2SO_4 samples (2 and 3). In contrast, the cation choline undergoes a greater decrease for 0.5 M salt than 1.0 M salt treatments, potentially suggesting that the cationic component is more susceptible to electrostatic disruption than the anion^{29,30}. For the trans-2-hexenoate anion (2-HA), a combination of electrostatics and hydrogen bonding seem to be equally crucial for its disruption^{31,32}. In particular, acid treatment after regular synthesis (0 M salt) induces the most loss, which then decreases to a minimum across the 0.5 and 1.0 M and acid treatments. In comparison, the amount of choline persists during both salt and acid treatments, along with its PLGA interfacial peaks between 3.5-4.0 ppm.

Interestingly, ‘masking’ of the PLGA’s PLA peak (at 2.0 ppm) is observed transitioning from 0 - 0.5 M salt. As bare PLGA nanoparticles are first synthesized and then resuspended in salt water for further stirring, the carboxylic acid surface modification is subject to modification and coating by the Na_2SO_4 , which is observed to extend to the 1.0 M salt treatment (Figure 1 A, line 3, green). Some PLA signal masking is also observed in the 0 M salt + acid treatment (Figure 1 A, line 4, teal), however not to the same degree as the 0.5 and 1.0 M salt + acid treatments (Figure 1 A, line 5 and 6), which are almost completely masked. This suggests that interference of surface electrostatics is critical to the mechanism of assembly.

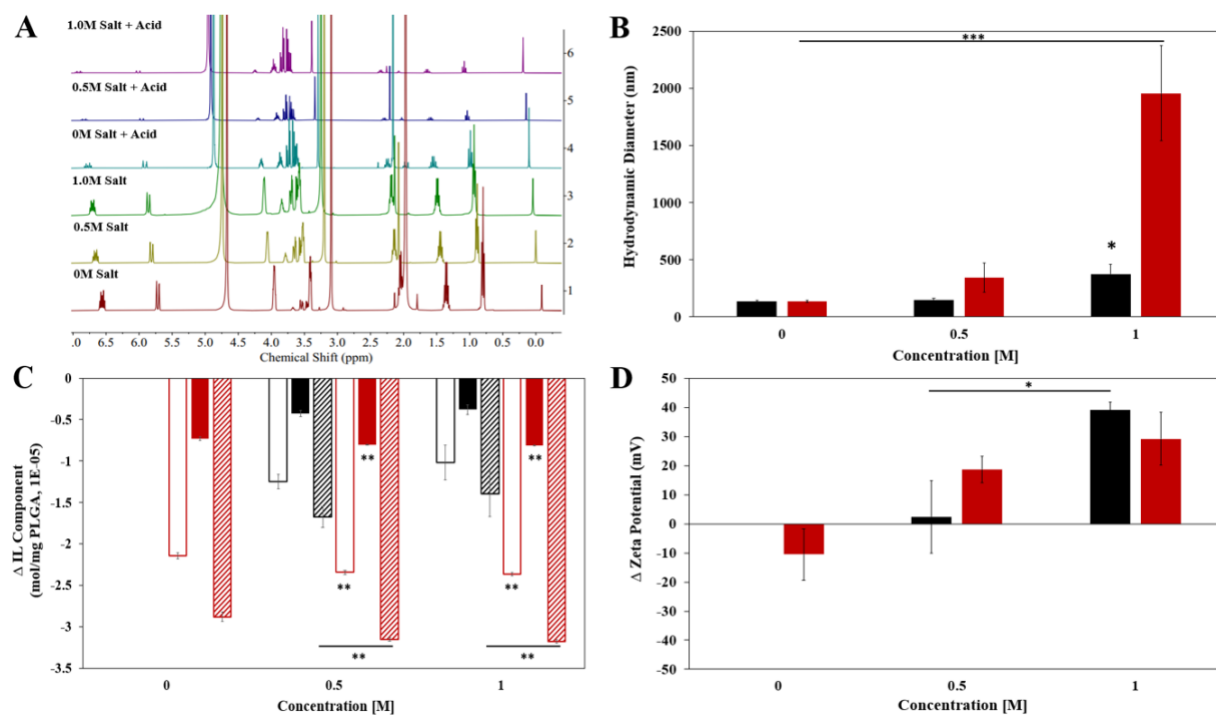


Figure 1. Both electrostatics and hydrogen bonding play a role in CA2HA 1:1-coated PLGA NP assembly (n = 3). (A) ^1H NMR spectroscopy in D_2O shows both salt (1-3) and acid (4) have a range of effects in reduction of IL peaks, with the most IL loss after both acid and salt treatments (5-6). (B) DLS shows 1.0 M salt (black) is sufficient to induce in IL-PLGA NP aggregation and hydrodynamic diameter increase, with the greatest increase from 1.0 M salt and acid titration (red). (C) Total quantified IL (0.9 and 3.1 ppm) loss ($\Delta\text{mol/mg PLGA}$) verify that both salt and acid are required for maximum disruption. 0 M untreated IL-PLGA NPs serve as a baseline with 0.2 mg DSS quantitative reference (1 mg polymer/500 μL). (D) DLS trends towards cationic shift on IL-PLGA NP surface charge at the higher salt concentrations (both with and without acid), represented as the change from 0 M untreated IL-PLGA NPs. Statistical comparison between two samples at a time represented as paired two-tailed t-test of the mean (n = 3), with ANOVA conducted across three or more samples as a time. * = $p < 0.05$, ** = $p < 0.01$, *** = $p < 0.001$. Color key: (B-D) black: salt (0-1M) treatment; red: salt (0-1M) and acid treatment; in addition, (C) color border: cation, color filled: anion, color striped: total IL.

Without protection from the CA2HA 1:1 IL coating, bare PLGA NPs that were originally assembled intact (no disruption during synthesis) and were then exposed to varying concentrations of salt water, or salt water with subsequent acid treatment, demonstrate a gradient of reduction in the PLA peak (~ 2.06 ppm) (Fig. S1A). When examining the precise change in PLA component of PLGA from quantitative ^1H NMR spectroscopy, a similar loss was found for both 0.5 M and 1.0 M salt treatments. Acid alone induced a similar loss to just salt treatments, with nonsignificant changes with acid treatment after salt titrations (Fig. S1C). It is possible that this peak masking is not loss of polymer, but instead suppression of signal by coating by Na_2SO_4 with additional deposition by protons and chloride ions after acid treatment³³.

This theory is possible because when ionic liquid is added after bare PLGA synthesis, 3 mL of water is required to disperse and distribute molecules of choline and trans-2-hexenoic acid, which then electrostatically assemble on the carboxylic acid –terminated PLGA surface during stirring over 2 hours. When observing shifts in NP size by DLS (Fig. S1B), bare PLGA NPs exposed to 0.5 M salt solution expand 6.6x, while the shift from 0 M to 1.0 M Na₂SO₄ expands nearly 49 times in size (ANOVA 0 M to 1.0 M; $p = 0.045$). While the ionic liquid has likely stronger interactions with the bare PLGA surface and tight electrostatic interactions between choline and 2HA, resulting in a compact nanostructure⁵, the electrostatics between sodium and sulfate may coordinate in a bulkier fashion, resulting in a larger and more unstable nanoparticle with some aggregation (PDI at 0 M = 0.14 ± 0.07 vs. PDI at 1.0 M = 0.90 ± 0.13)³⁴. In contrast, treatment with acid after salt similarly increases the hydrodynamic diameter (HD) of the bare PLGA NPs at all salt concentrations (although with large variance, likely from particle instability), possibly both from new deposition of hydrogen and chlorine molecules, as well as removal of sulfate molecules at the outermost surface at 0.5 M and 1.0 M, contributing to potential solvent penetration³⁵ as well as high nanoparticle aggregation (0 M + acid PDI = 0.66 ± 0.34 ; 0.5 M + acid PDI = 0.84 ± 0.21 , 1.0 M + acid PDI = 0.79 ± 0.28).

Interestingly, the corresponding surface charge of the bare PLGA NPs (0 M = -20.50 ± 4.40 mV) seems to shift continuously towards an anionic charge with increasing salt concentration, suggesting the sulfate is also assembled on the outside with the anionic component of IL-PLGA NPs (1.0 M = -33.40 ± 3.30 mV) (Fig. S1D). In contrast, acid treatment of bare PLGA NPs appears to add a cationic component (-1.10 ± 7.10 mV), verifying the deposition of protons to neutralize the carboxylic acid –terminated surface. With the addition of acid after each salt treatment, the surface charge shifts more positively, however on a decreasing trend compared to the 0 M control. In the case of acid treatment after the 0.5 M (-8.9 ± 7.0 mV) and 1.0 M (-15.0 ± 3.50 mV) salt titrations, the overall change in zeta potential may be indeed from the removal or masking of the sulfate ion (which has a -2 charge) with protons and replacement by chloride anions (which have a -1 charge), contributing to the overall cationic shift, with additional reduction in surface stability.

When examined by Dynamic Light Scattering (DLS) in Figures 1B and D, IL-PLGA NP size does not increase between non-disruptive synthesis (0 M Na₂SO₄) and 0.5 M salt treatment ($p = 0.48$), while the hydrodynamic diameter expands from 0 M by nearly 2.8 times with 1.0 M salt treatment ($p = 0.025$). This can be attributed to the high concentration of salt present in the system which can modify the bare PLGA NPs, before the IL assembles on the surface, in the IL coating itself, and on its surface, thereby both expanding the diameter of the particles, as well as masking the PLA's proton signals by NMR spectroscopy. In contrast, acid treatment after regular synthesis (0 M salt) seems to not affect the size of IL-PLGA NPs, maintaining a nearly identical size distribution profile (Table S1). However, exposure to acid after 0.5 M salt treatment increases the 0 M NP diameter by nearly 2.5 times, which further increases at 1.0 M by ca. 14 times in magnitude relative to the 0 M untreated control (ANOVA, $p = 6.69 \times 10^{-7}$). It is possible that the salt treatment

interferes with the supramolecular organization of the IL at the PLGA interface, allowing for its removal with acid after salt treatment and thereby destabilizing the NPs and inducing aggregation.

In parallel, the addition of 0.5 M Na₂SO₄ to IL-PLGA NPs results in greater instability and a positive zeta shift, becoming drastically more pronounced from 0.5 M to 1.0 M ($p = 0.034$). While IL-PLGA NPs typically demonstrate a very anionic surface potential ($n = 3$, -59.5 ± 6.18 mV), the positive shift may be in part due to the ability of the salt to integrate into, assemble on, and neutralize the surface of the IL coating. At 1.0 M Na₂SO₄, 40.28 ± 8.1 % total IL is lost from the native system ($1.40 \pm 0.3 \times 10^{-5}$ mol/mg PLGA). In contrast, much more IL is comparatively lost at 0.5 M Na₂SO₄ (48.12 ± 3.5 %) than at 1.0 M, albeit this is not statistically significant ($p = 0.33$). The greater loss of IL at 0.5 M may contribute to a more unstable surface with the large error observed, while the sheer abundance of salt in the 1.0 M treatment amplified the modified surface density of adsorbed salt components (such as Na⁺ ions).

Furthermore, once acid treatment was incorporated, the surface charge immediately shifted more negatively for 0 M IL-PLGA NPs (-69.9 ± 2.7 mV). The loss of IL transitioning from 0 M to 0 M + acid is even more dramatic (83 ± 2 %), but IL is still strongly present in the NP system by NMR spectroscopy, it is possible that Na⁺ and SO₄²⁻ ions are instead replacing 2-HA and choline's charged assembly branching outwards and are thus restabilizing the PLGA surface coating. However, as more IL is lost from the system with 0.5 M Na₂SO₄ + acid (90.6 ± 0.7 %) and 1.0 M Na₂SO₄ + HCl (92 ± 1 %), the surface charge instead shifts towards a cationic charge. Two possible scenarios are consistent with the NMR spectroscopy: (1) Either enough IL has been removed down to the cationic interfacial coating layer, and instability from drastic loss of IL induced mass aggregation and thus a strongly cationic surface, or (2) That because of the PLA peak masking observed, that IL is removed down to the interfacial layer and replaced by salt components, with Na⁺ strongly driving composition of the external interfacing layer of the salt coating.

To confirm these observations by examining the precise amounts of IL components lost relative to the native synthesis (0 M salt, 0 M acid) of IL-PLGA NPs (Figure 1C), anionic loss between 0.5 M and 1.0 M salt appears to be consistent and doesn't significantly change ($p = 0.46$). In contrast, cationic loss with salt treatment appears to be the largest in magnitude at 0.5 M salt and tapers with doubling the salt concentration, albeit with no statistical difference between 0.5 and 1.0 M salt ($p = 0.30$), resulting in a comparative amount of total IL loss between 0.5 - 1.0 M salt treatments ($p = 0.33$). However, when treated with acid after 0.5 M salt, anionic content of 2-HA was seen to significantly decrease, approximately 2-fold ($p = 0.0028$), with 2.14 times decrease at 1.0 M salt ($p = 0.0062$). Although with a smaller relative decrease at 0.5 M ($\sim 1.85x$) and a larger relative decrease at 1.0 M ($\sim 2.3x$), this trend was also observed for choline at 0.5 M ($p = 0.0030$) and 1.0 M ($p = 0.0067$) after acid treatment. Both the amount of anion loss and cation loss was not further observed to significantly increase between acid-treated 0.5 M and 1.0 M samples ($p = 0.18$ and $p = 0.23$ respectively). However, when acid was treated after regular synthesis (0 M), anion

loss was significantly less than when first salt treated (0 M + acid vs. 0.5 M + acid, $p = 0.026$), which was also observed for cation loss (0 M + acid vs. 0.5 M + acid, $p = 0.025$), leading to total loss of IL being statistically significantly less at 0 M than 0.5 M when acid treated afterwards ($p = 0.025$). This suggests that without initial interference and destabilization of electrostatics, both anionic and cationic components within CA2HA 1:1 are less sensitive to disruption and the removal of hydrogen bonding alone during the IL assembly mechanism to coat PLGA NPs.

Similar to IL-PLGA NPs, electrostatics and hydrogen bonding are both important in the assembly of the IL on the EPP NPs. For the treatment with HCl alone, acid had little effect on the structural form of the EPP NPs, which is shown by minimal size and charge differences (Figures 2B and D) between native NPs and acid titrated systems. Despite this occurrence, there was a significant drop in the IL coating of $94 \pm 2.1\%$ ($p = 0.041$). In the presence of 1.0 M Na_2SO_4 , there was more than 100-fold increase in size ($8.3 \pm 0.5 \times 10^3$ nm) compared to the native coated EPP NPs (74 ± 0.7 nm) and to the acid only NPs (78 ± 8 nm), both with $p = 0.0012$. However, interestingly, 0.5 M decreased the amount of IL coating similarly to 1.0 M of salt, with the amount of IL being the same within error at $54 \pm 17\%$ and $36 \pm 43\%$, respectively (Figures 2A and C). This indicates that at high quantities of Na_2SO_4 , there is little difference in the salt's impact on preventing the IL from interacting with the EPP NPs. Despite an appreciable change in size (100-fold increase) and charge (23 ± 13 mV increase) at 1.0 M salt, there is no notable effect of salt on the interactions of the IL with the NPs, as evidenced by comparison of the loss of the IL with adding acid after salt titration ($100 \pm 0.4\%$) compared to acid alone ($97 \pm 2\%$).

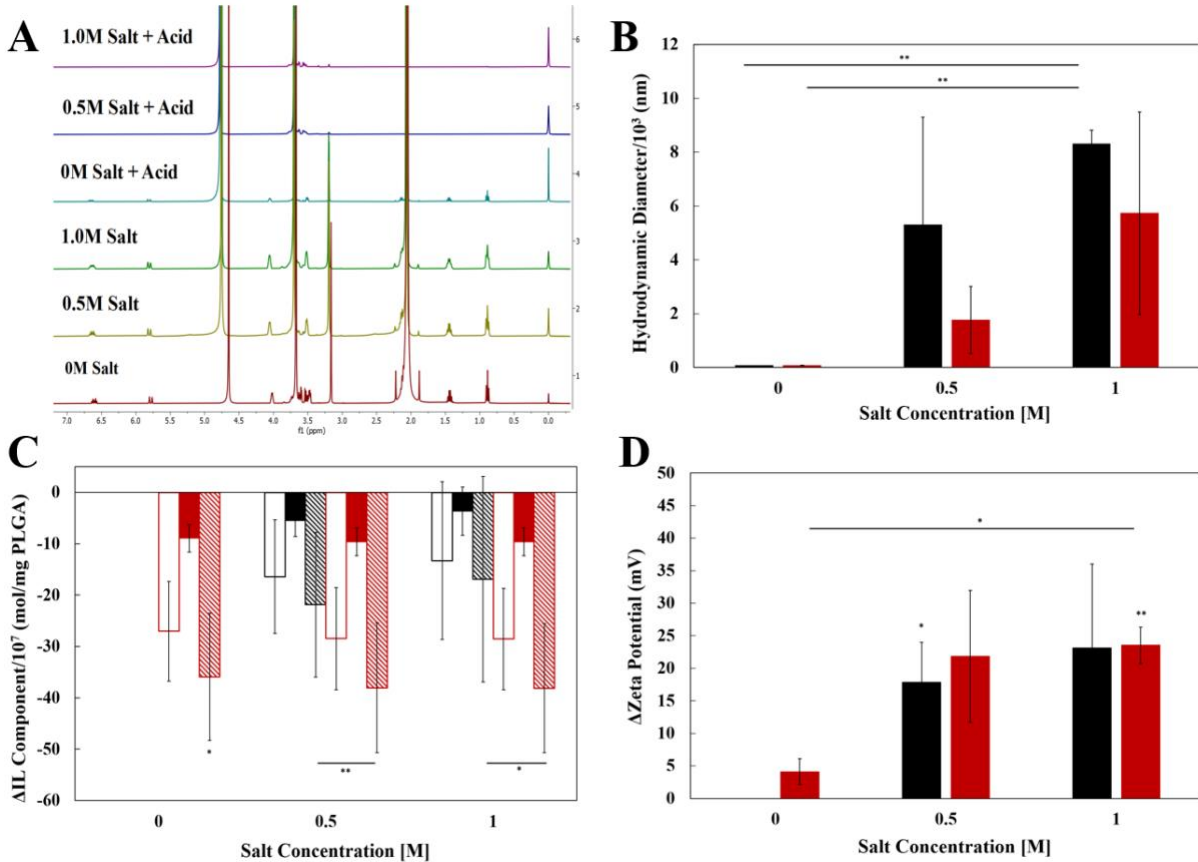


Figure 2: Both electrostatics and hydrogen bonding participate in CA2HA 1: 1 coating abilities on electrostatically bound PLGA PEG NPs. (A) The overlaid ^1H NMR spectra in D_2O shows the reduction in IL (0.9 and 3.2 ppm) and polymer peaks (2.0 and 3.7 ppm) with salt (1-3) showing little change in IL while acid (4) shows much more loss. (B) The DLS shows the hydrodynamic diameter increasing drastically with the addition of salt. (C) The total loss in cation, anion, and total IL based on the 5 mg of PLGA used and relative to native EPP IL NPs shows much more loss in IL after acid titration. (D) The DLS shows the increase in zeta potential (charge) relative to the native EPP IL NPs with not much difference between all the salt titrations. The change in charge is mostly seen when comparing native coated or acid titrated EPP NPs to the other conditions. Comparing the native coated particles to either 0.5 M of Na_2SO_4 or 1.0 M salt plus acid, $p = 0.037$ and $p = 0.046$, respectively. In addition, there was a significant difference in charge with the acid titrated EPP NPs and the 1.0 M of salt plus acid ($p = 0.012$) Black represents only salt titrated. Red represents salt plus acid titrated. No fill is the cation (Choline). Solid fill is the anion (2-hexenoate). Diagonal striped fill is total IL (cation + anion). Statistics were performed with paired two-tail tests using $p < 0.05$, $n = 3$, and ANOVA. * = $p < 0.05$ ** = $p < 0.01$, and *** = $p < 0.001$.

Although 0.5 M or 1.0 M of Na_2SO_4 plus HCl decreased the amount of IL coating on EPP by 99 ± 0.2 and $100 \pm 0.3\%$, respectively, HCl alone was $94 \pm 2\%$. This indicates that the addition of salt is needed to completely remove the IL from the NPs, but the order does not matter. Acid has a greater effect on the IL coating than the salt, supporting the notion that hydrogen bonding plays

a more significant role in the interactions between the IL and the EPP NPs. However, there are still some electrostatic interactions present that are disrupted by the salt.

In addition, the acid and 1.0 M separately appear to affect the polymers of the NPs a little more than at 0.5 M by NMR spectroscopy. The loss of PLGA and PEG with acid is $99 \pm 0.2\%$ and $99 \pm 0.16\%$, respectively, while at 1.0 M it is $89 \pm 11\%$ and $82 \pm 13\%$. At 0.5 M, it was $91 \pm 3.2\%$ and $91 \pm 2.5\%$. For uncoated EPP NPs, acid alone had a smaller influence on the loss of polymer with values of $9.2 \pm 16\%$ for PLGA and $31 \pm 29\%$ for PEG (Fig. S9C). However, there was still a substantial loss in both polymers when salt was added at both concentrations. 0.5 M Na_2SO_4 decreased the amount of PLGA by $99 \pm 0.7\%$ and PEG by $89 \pm 9\%$. 1.0 M Na_2SO_4 resulted in a decrease of $99 \pm 0.7\%$ for PLGA and $91 \pm 3\%$ for PEG. When acid titration was performed after salt titration for both concentrations, PLGA polymer was completely lost despite the little amount of PEG still present. Therefore, there was more of an impact to the polymers in the uncoated NPs with acid after salt titration. This shows that the electrostatically bound PEG may have helped to protect the PLGA from hydrolysis, acting as a shield from the acidic environment. After salt titration, with the decrease in PEG coating, the strength of this shield is decreased, allowing the hydrolysis of PLGA to occur.

For NP systems, IL is normally used as a (second) layer of protection from the environment or as a stabilizing tool for NPs. Thus, like the PEG, it should protect the PLGA from being degraded. Instead, it acts as a catalyst because of the hydrogen bonding between the PEG and IL. As these bonds are disrupted, it pulls the PEG away from PLGA, destabilizing the NPs in general, and allowing PLGA to undergo hydrolysis once placed in an acidic environment. Therefore, in EPP NP IL systems, both salt and acid have a huge effect on their durability. However, it takes extreme conditions for full disruption of IL interactions with the EPP NPs. This indicates that environments with a low salt concentration (such as 1x PBS) and higher pH conditions (> 4.8) there would be less of an affect in the loss of CA2HA 1: 1 and the stability of these NPs.

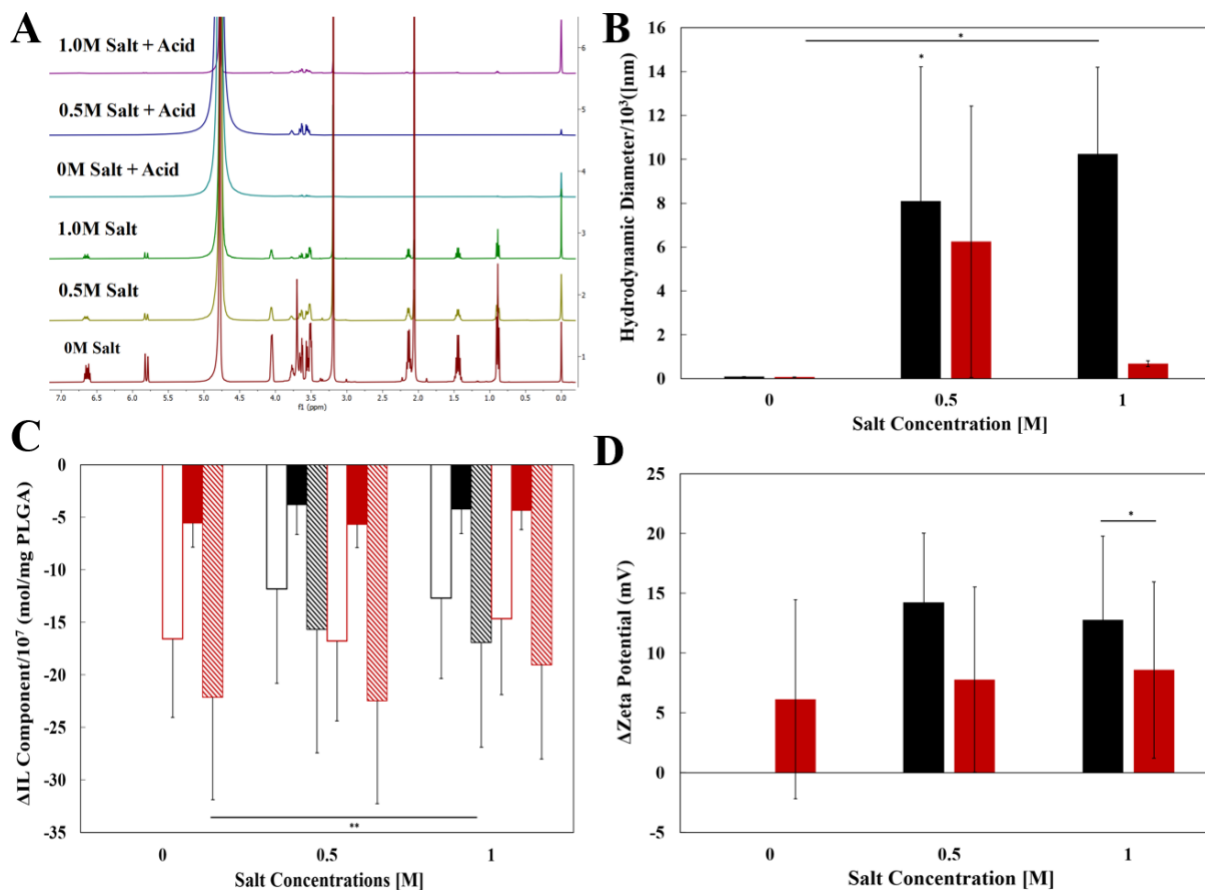


Figure 3. Hydrogen bonding plays a big role in the assembly of CA2HA 1: 1 on the diblock copolymer, PEG-b-PLGA. (A) ^1H NMR spectroscopy in D_2O shows little loss of IL after salt titration (1-3) with acid almost decreasing it to none. **(B)** DLS displays minimal increase in hydrodynamic diameter after all acid titrations but a substantial increase after salt addition. **(C)** IL loss shown mostly with acid with little difference after salt or without salt. **(D)** DLS shows no change in charge with the addition of acid without or after salt titration with a cationic shift with salt addition. Black represents only salt titrated. Red represents salt plus acid titrated. No fill is the cation (Choline). Solid fill is the anion (2-hexenoate). Diagonal striped fill is total IL (cation + anion). 0.2 mg DSS was used as a quantitative reference in the ^1H NMR spectroscopy. Statistics were performed with paired two-tail tests using $p < 0.05$, $n = 3$, and ANOVA. * = $p < 0.05$ ** = $p < 0.01$, and *** = $p < 0.001$.

On the other hand, hydrogen bonding plays more of a role in IL coating on DPPs. For the DPPs represented in Figure 3A, salt treatment with 0.5 M and 1.0 M have a similar effect on both the choline and 2-hexenoic components of the IL coating on the particles shown with similar decreases in their peaks (3.2 and 0.98 ppm, respectively). This is reinforced with Figure 3C showing that the change in IL components is similar and their calculated decrease in the amount of IL present was $59 \pm 36\%$ for 0.5 M and $69 \pm 18\%$ for 1.0 M. Like with the EPP IL NPs, the amount of salt, at high concentrations, disrupts the IL's interactions with the polymer to the same degree. However, also seen in these figures, acid alone has more of a significant impact on the IL's capabilities to coat the NPs than just salt ($p = 0.049$ for 0.5 M, $p = 0.0011$ for 1.0 M) with a greater decrease in IL.

The acid alone can prevent the IL from coating just as much as the salt alone. This could be due to the acid hydrolyzing the PLGA since its peak is not shown in the ^1H NMR spectrum (Fig. S12A) while in the spectra for the salt treatments, there is still about 7-13% PLGA not degraded and attached to PEG. Although, once the salt titrated NPs are treated with acid, the IL is completely removed with the 0.5 M treated NPs and mostly gone with the 1.0 M treated NPs. The PLGA peak is also gone. This indicates that the PLGA component of the diblock co-polymer is important to the IL being able to coat the particles in that the core particles must be stable to enable to coating to persist.

Despite acid alone having a great impact on IL coating, it has no effect on the DPP NPs HD (Figure 3B). As the acid hydrolyzes the PLGA polymer, the particles keep their structure as if it is only creating holes in the sphere with little difference in its charge (Figure 3D). When the particles are salt titrated with either 0.5 M or 1.0 M Na_2SO_4 , however, the size increases substantially with 1.0 M having a significant difference to both the DPP IL NPs and the acid titrated NPs ($p = 0.047$). At this point, the HD decreases to almost the same size as DPP IL NPs and the acid-only treated NPs. Like with the EPP NPs, the salt weakened the interactions between the IL and the DPP NPs, but some of the IL is still loosely bound to the particles. Thus, the loosely bound IL increases the hydrodynamic diameter of the particles, before the acid comes in and knocks the remaining IL off the surface of the NPs, bringing the size down.

The charge of the salt treated particles becomes more positive compared to the non-salt condition. This could indicate that there is a layer of sodium ions layering the outside of the NPs, that salt disrupted the layering of the particles so that bulk of the outside layer is choline, the cation, or that with the loosely bound IL, the parts of the IL rearranged itself to show the cation on the outside in order to stay on the particles. When the acid comes in disrupts the interactions occurring with the IL and the NPs, the size might change with the salt treated NPs, but the difference in charge change is insignificant for all the acid treated NPs compared to the salt treated NPs and the coated DPP NPs. This reveals that when PLGA is absent, the PEG that is left may have rearranged itself to preserve the NP structure.

As for bare DPP NPs, when they are titrated with either salt, acid, or a combination, there is no significant difference in the change in the PLGA peak (Fig. S12A) between all the treated ones. However, there is a great difference when comparing them to the native bare DPP NPs. They all have $92 \pm 0.4\%$ to $99 \pm 2\%$ decrease in PLGA while there is more of a variance in the loss of PLGA for the coated DPP NPs, especially for 1.0 M with acid ($63 \pm 61\%$). With no IL, the salt and acid does not impact the structure of the bare NPs (Fig. S12B) at 0 M or 0.5 M. It is not until 1.0 M of salt and acid that the HD increases substantially ($p = 0.0041$) and the change in surface charge (Fig. S12D) is significantly impacted compared to the native bare NPs ($p = 0.048$) and the 1.0 M only ($p = 0.00067$). This reveals that in the presence of IL, there is a wide variance in the

way that the polymers of the NPs are affected, especially at 1.0 M salt and acid, sometimes allowing the NPs to stay intact.

When compared to the other systems, the IL-LDBC proton NMR spectrum in Figure 4A instead shows that salt treatment on its own has little-to-no impact on the amounts of 2-hexenoic acid and choline within CA2HA 1: 1. Instead, after exposure to 0.5 M salt during synthesis, the area under the peak appears to increase, indicating that masked areas within the IL-polymer graft containing cation and anion may be reorganizing and being exposed from the graft, increasing their proton signal. In comparison, disruption of the IL-LDBC assembly by 1.0 M salt treatment induces a greater loss of cation than anion (however, both in comparable amounts ‘released’ from the graft at 0.5 M Na₂SO₄), potentially suggesting that the dominant interactions for the cation within the bulk of the IL-LDBC dendritic graft favor distance-ranged electrostatic interactions³⁶, which requires at least 0.5 M of salt to weaken and be released at 1.0 M Na₂SO₄. However, upon acid treatment of the 0 M native synthesis with 0.25 M HCl, the most significant loss of both 2-HA and choline is observed, which only incrementally increases when 0.5 M and 1.0 M salt treatments preceded the acid treatment. This outcome may suggest that while electrostatic disruption played a role in ‘fluidizing’ the graft, disruption of pure hydrogen-bonding is required to separate the most anionic component from the NH₃⁺ terminated dendritic interface, which then allows the most IL to leave the system^{37,38}.

In contrast to the masking effect observed for PLGA’s PLA peak during both salt and acid titrations, LDBC PAMAM peaks become more pronounced (4.0 x for 0.5 M salt, 4.75 x for 1.0 M salt), and emerge from the graft (Fig. S5) as the electrostatics are weakened between the IL and polymer. In contrast, when hydrogen bonding between the IL and polymer is disrupted *after* salt treatment on the same samples, PAMAM peaks become less exposed (0 M + acid: 0.61x; 0.5 M + acid: 2.0x; 1.0 M + acid: 2.25x). This may be in part due to replacement of anion at the NH₃⁺ dendritic interface with chloride anions from HCl, which mask the PAMAM protons during removal of IL.

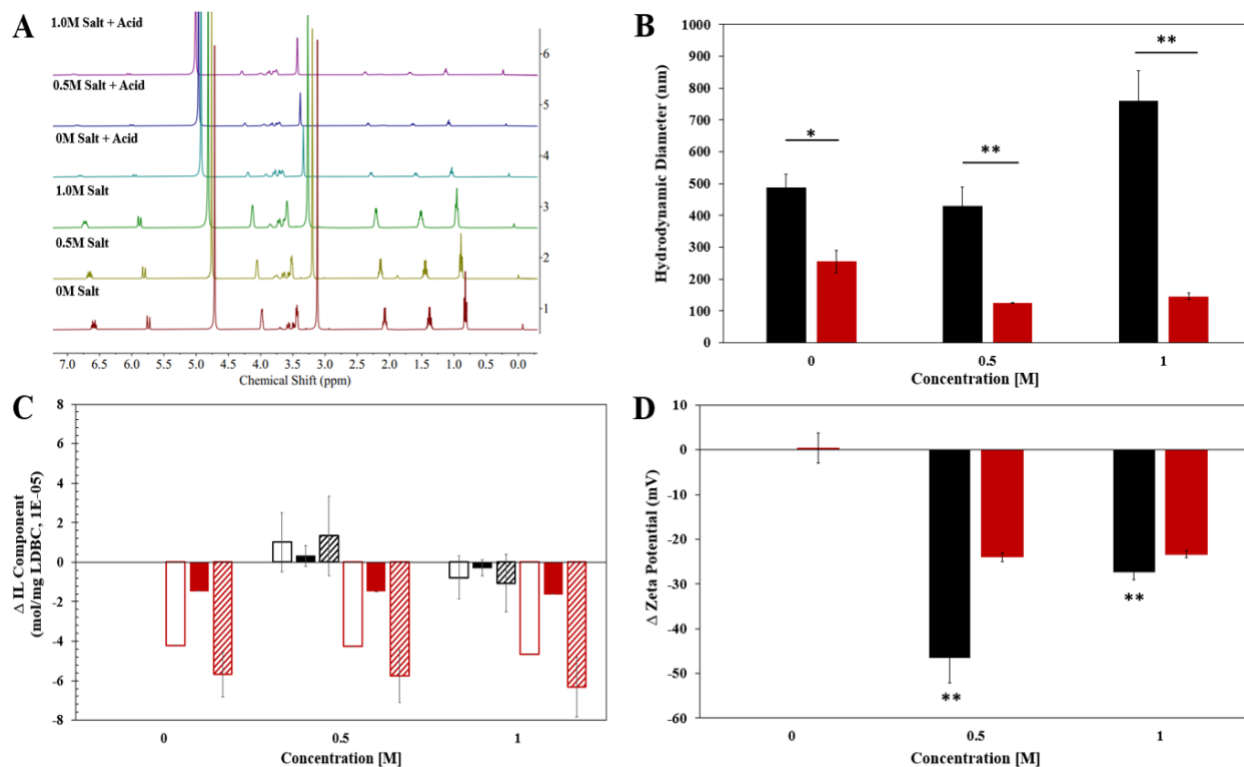


Figure 4. While electrostatics play a role in outer IL-LDBC formation, hydrogen bonding predominantly drives bulk assembly in CA2HA 1: 1-coated LDBC NPs (n = 3). (A) ^1H NMR spectroscopy in D_2O displaying minimal IL loss after salt (1-3), with the most loss after acid (4), or acid and salt combination treatments (5-6). (B) DLS only shows a decrease in IL-LDBC hydrodynamic diameter after acid and salt and acid titration, consistent with IL loss seen by NMR spectroscopy. (C) Similar loss of IL content (0.9 ppm and 3.1 ppm) ($\Delta\text{mol/mg LDBC}$) is observed between acid only and salt and acid treatments, suggesting disruption in hydrogen bonding is the ultimate determinant of disruption. 0 M untreated IL-LDBC NPs as a baseline with 0.2 mg DSS quantitative reference (1 mg polymer/500 μL). (D) DLS shows anionic shifts in the surface charge of IL-LDBC NPs from salt (black) or salt and acid (red) titration, represented as the change from 0 M untreated IL-LDBC NPs. 0.2 mg DSS was used as a quantitative reference in the ^1H NMR spectroscopy. Statistical comparison between two samples at a time represented as paired two-tailed t-test of the mean (n = 3), with ANOVA conducted across three or more samples as a time. * = $p < 0.05$, ** = $p < 0.01$, *** = $p < 0.001$. Color key: (B-D) black: salt (0-1M) treatment; red: salt (0-1M) and acid treatment; in addition, (C) color border: cation, color filled: anion, color striped: total IL.

DLS reveals that the IL-LDBC hydrodynamic diameters between the native (0 M) IL-LDBC synthesis and the two salt treatments did not significantly change (0 M vs. 0.5 M Na_2SO_4 , $p = 0.07$; 0 M vs. 1.0 M Na_2SO_4 : $p = 0.056$). However, the addition of acid after 0 M salt synthesis reduces the 0 M IL-LDBC size almost two-fold (1.91x, $p = 0.02$), which also significantly decreases between 0.5 M to 0.5 M + acid ($p = 0.006$) and 1.0 M to 1.0 M + acid ($p = 0.0049$) combined treatments. Overall, treatment with 0.5 M salt + acid reduces the 0 M untreated IL-

LDBC control diameter by 3.9x ($p = 0.006$), with the size remaining comparably low ($p = 0.08$) between 0.5 M and 1.0 M salt + acid treatments. As the addition of Na_2SO_4 disrupts the electrostatics of the intermolecular interactions governing the cation, anion, and LDBC, rearrangement of the IL and polymer can be explained by the NP diameter transition from 0 M to 0.5 M salt. In contrast, IL loss at 1.0 M is responsible for the increase in size due to aggregation or less tightly organized nanostructures. However, in line with the steep loss of IL between the 0 M salt and 0 M salt + acid samples, interference of hydrogen bonding primarily participates in cleaving/removal of IL, thereby reducing the size as it continues to extract away from the polymer interface.

When examining the change in zeta potential in tandem with NP size measurements, almost no difference is observed between 0 M salt and its subsequent acid treatment ($p = 0.84$). This could be due to the equal loss of cation ($80.9 \pm 4.5\%$) and anion ($80.6 \pm 4.3\%$) occurring at the IL-polymer interface, leading to minimal change of total surface charge. However, with increasing loss of total IL at 0.5 M + acid ($82 \pm 3\%$) and 1.0 M + acid ($89 \pm 2\%$), the native IL-LDBC surface charge (34.1 ± 0.86 mV) significantly transitions towards neutrality after 0.5 M Na_2SO_4 and acid treatment (10.1 ± 0.75 mV, $p = 0.00053$), completing a similar transition after 1.0 M Na_2SO_4 and acid treatment (0.5 M vs. 1.0 M Na_2SO_4 ; $p = 0.20$). In contrast, native IL-LDBC disruption by 0.5 M Na_2SO_4 alone induces a significant shift in surface charge towards an anionic state (-12.6 ± 6.8 mV, $p = 0.0046$). However, when treated by 1.0 M Na_2SO_4 , the IL-LDBC surface instead shifts towards cationic neutrality ($p = 0.0012$). Interestingly, as IL-LDBC size doesn't significantly change between 0 M and 0.5 M salt treatments, the drastic anionic shift in surface potential verifies IL rearrangement (0.5 M) at the polymer surface before minimal removal (1.0 M, $12.1 \pm 19.7\%$ total IL loss), which possibly explains the significant change between the two Δ values therein ($p = 0.024$).

When examining the precise amounts of IL components lost from untreated (0 M) IL-LDBCs, Δ anion loss ($p = 0.80$), Δ cation loss ($p = 0.83$), and Δ total IL loss ($p = 0.82$) did not significantly change between acid treatment alone after synthesis (0 M + acid) vs. 0.5 M and 1.0 M salt titration during synthesis with acid treatment afterwards, supporting observations that Hydrogen-bonding alone drives the most loss of IL from the IL-LDBC system. Consistent with DLS and NMR spectra observations, when treated with 0.5 M Na_2SO_4 , the total amount of detectable IL in the system increases (Δ IL gain: $1.33 \pm 2 \times 10^{-5}$ mol IL/mg LDBC), particularly for the cationic component (Δ cation gain: $1.01 \pm 1.5 \times 10^{-5}$ mol choline/mg LDBC) over anion, although not this is not statistically significantly different ($p = 0.35$). The observed IL loss at 1.0 M Na_2SO_4 however, is consistent with the amount gained at 0.5 M Na_2SO_4 (Δ cation: $1.01 \pm 1.5 \times 10^{-5}$ mol/mg gain vs. $-0.8 \pm 1 \times 10^{-5}$ mol/mg loss, Δ anion: $3.2 \pm 5 \times 10^{-6}$ mol/mg gain vs. $2.9 \pm 3.90 \times 10^{-6}$ mol/mg loss, Δ total IL: $1.3 \pm 2.02 \times 10^{-5}$ mol/mg gain vs. $1.06 \pm 1.47 \times 10^{-5}$ mol/mg loss).

Without CA2HA 1: 1 IL, however, peaks corresponding to the PAMAM and PCI protons from bare LDBC appear to have no significant change from electrostatic disruption during synthesis (Fig. S2A) but are heavily decreased in signal when treated with hydrochloric acid, which works directly to disrupt the hydrogen bonding at the NH_3^+ -terminated dendritic interface, as well as with the covalent bond between PAMAM and PCI (Fig. S2C). When examining changes in size from DLS (Fig. S2B), bare LDBCs steadily increase both in size (ANOVA 0 M-1.0 M, $p = 7.7 \times 10^{-6}$) and PDI when exposed to 0.5 M (2.6x larger, $p = 0.009$, 0.74 ± 0.10 PDI) and 1.0 M (4.2x larger, $p = 0.004$, 0.77 ± 0.12 PDI) Na_2SO_4 during assembly. This effect is likely not from electrostatic disruption but rather aggregation in the presence of charged sodium and sulfate molecules, which the PCI-PAMAM- NH_3^+ 50: 50 formulation has a tendency towards when assembling in water alone (0 M PDI = 0.54 ± 0.18)¹³. While 0 M bare LDBCs remain very similar in size when acid treated, there seems to be an overall trend of size decrease (non-significant) when 0.5 M and 1.0 M salt titrated bare LDBC are treated with acid. This may be possibly due to disruption of hydrogen bonding at the dendritic PAMAM interface, both causing removal of salt molecules, as well as breaking apart nanoaggregates.

Interestingly, the highly cationic outer surface charge, due to NH_3^+ termination at the PAMAM dendritic interface (54.6 ± 2.1 mV), is observed to neutralize very similarly compared to acid treatment alone (likely from disruption of hydrogen bonding and chloride anion coordination) as when salt is added to the system (0.5 M vs. 1.0 M, $p = 0.16$), and both salt and acid (0 M vs. 1.0 M, $p = 0.17$) are added to the system. This suggests that surface modification by hydrogen, chloride, sodium, and sulfate molecules may be working similarly to mask the LDBC interface, either by likely depositing chloride (acid alone) or sulfate molecules (salt alone) onto the NH_3^+ moieties, or disruption of formed hydrogen bonds (a new peak at 1.1 ppm forms with 0.5 M salt and acid that then diminishes at 1.0 M salt and acid) by hydrochloric acid with electrostatic replacement by chloride ions at the NH_3^+ interface³⁹.

Conclusions

We show that in each polymer-based NP system, electrostatics and hydrogen bonding influences the coating abilities to different degrees. With no significant difference in loss of CA2HA 1: 1 without initial interference with salt, electrostatics and hydrogen bonding are both essential for the assembly of this IL on PLGA NPs. On the other hand, EPP NPs shows more of a loss in IL with acid treatment alone, but its coating was still not completely disrupted. This shows that hydrogen bonding plays a little more of a role in coating EPP NPs, but electrostatics are still important. For DPP NPs and LDBCs, hydrogen bonding displayed a more substantial role in the assembly of the IL coating with much higher disruption being observed when using acid alone. However, the hydrogen bonding in the IL-LDBCs is much stronger than they are within the IL-DPP NPs, represented by still-present IL peaks after salt and or acid treatment. Despite knowing the level at which these interactions exist, the specific layers of ionic liquid created on these NPs and the

specific molecular interactions occurring between the solvent, IL, and NP surface is still unknown, necessitating future studies by Atomic Force Microscopy (AFM), small angle neutron (SANS) and x-ray scattering (SAXS).

Materials and Methods

IL Synthesis: The ionic liquid choline and trans-2-hexenoic acid (CA2HA) was synthesized as previously published¹³. Briefly, choline bicarbonate (80% v/v in water) (Sigma Aldrich, #C7519-500 ML) was combined with 95% pure trans-2-hexenoic acid (Sigma Aldrich, #W316903-1KG-K), at a 1: 1 ratio, in a 500 mL round bottom flask and stirred for 24 hours at 40°C, dried by rotary evaporation at 60°C and 15 mbar for 2 hours, and vacuum dried at -760 mmHg (60°C) for 48 hours. The final product (MW: 218.31 g/mol, yield: 81.9%, density: 1.56 g/cm³) was characterized by ¹H NMR spectroscopy (400 MHz, DMSO) δ 6.30 (dt, *J* = 15.5, 7.0 Hz, 1H), 5.64 (dd, *J* = 15.5, 1.6 Hz, 1H), 3.84 (dq, *J* = 7.8, 2.7 Hz, 2H), 3.50 – 3.45 (m, 2H), 3.16 (s, 9H), 2.03 – 1.96 (m, 2H), 1.40 – 1.32 (m, 2H), 0.85 (t, *J* = 7.4 Hz, 3H), and Karl Fischer titration (1.22% wt/wt).

IL-PLGA NP Synthesis: IL-PLGA NPs were synthesized as described by nanoprecipitation as described previously⁴. Briefly, 1 mg/mL organic phase of Resomer 504H PLGA 50: 50 (carboxylic acid terminated, 38-54 kDa) (#719900-5G) in HPLC-grade Acetonitrile (Sigma Aldrich, #34851-4L) was combined dropwise with an aqueous phase of 3 mL D₂O water (Sigma Aldrich, #435767-1KG) stirring at 1200 RPM and solvent evaporated for 3 hours at 25°C. Ten mg neat IL/mg PLGA was then added as 1 drop to the bare NP solution stirring at 800 RPM for 1 hour, and an additional 1 hour at 900 RPM (2 hours total). Finally, IL-PLGA NPs were centrifuge-filtered at 2500 RPM (Thermo Scientific Sorvall Ultracentrifuge, #ST8R), 1 hour at 4 °C in 4 mL Amicon 30 kDa filter tubes (Sigma Aldrich, #UFC803096). For storage, filtrates were resuspended to 1 mg/mL in D₂O and stored at 4°C for up to 3 weeks. For measurement, filtrates were resuspended to a final volume of 500 μL D₂O for quantitative ¹H NMR spectroscopy with 0.2 mg deuterated 3-(trimethylsilyl)-1-propanesulfonic acid (DSS-d₆) sodium salt (Cambridge Isotope Laboratories, Inc., MA, USA, DLM-8206-1). The 500 uL was brought up to 1 mL in D₂O for dynamic light scattering (DLS) measurements of hydrodynamic diameter, zeta potential, and polydispersity.

IL-PLGA NP Salt Titration: Bare PLGA NPs were synthesized as described above, and gently centrifuge filtered at 2000 RPM for 30 minutes at 4°C. Bare PLGA NP filtrate (200-300 μL) was then recombined to the original volume of 3 mL in an aqueous phase containing 0, 0.5 M, or 1.0 M Na₂SO₄ salt (Sigma Aldrich, #239313-500G) and allowed to stir for 2 minutes to redisperse within the solution. IL was then added at the same specifications, the solution stirred for 2 hours, and the filtration procedure was followed, exactly as described above. One mg filtrate was resuspended to 500 μL with D₂O for quantitative ¹H NMR spectroscopy with 0.2 mg DSS, which was then afterwards brought up to 1 mL for DLS measurements (no additional dilution to preserve entire sample). A control salt titration was conducted with bare PLGA NPs after synthesis where the above protocol was followed, but without the addition of IL, with identical stirring and filtration steps. All titrations were performed in triplicate.

IL-PLGA NP Acid Titration After Salt: Bare and IL-PLGA NPs were synthesized and salt titrated as described above. After ^1H NMR spectroscopy and DLS characterization, all NPs were gently centrifuge- filtered at 2000 RPM for 30 minutes at 4°C . Reconstituted Bare or IL-PLGA NP filtrates (200-300 μL) were then recombined to a final volume of 3 mL with an acidic D_2O phase at pH 4.8 titrated with 0.25 M HCl (Sigma Aldrich, #320331-2.5L). NP solutions were allowed to stir for 2 minutes to redisperse the NPs within the acidic water. For IL-PLGA NPs, IL was then added at the same specifications, the solution stirred for 2 minutes (1 minute at 800 RPM, 1 minute at 900 RPM), and the filtration procedure was followed, exactly as described above. One mg filtrate was resuspended to 500 μL with D_2O for quantitative ^1H NMR spectroscopy with 0.2 mg DSS, which was then afterwards brought up to 1 mL for DLS measurements.

IL-EPP NP Synthesis: IL-EPP NPs were synthesized through a modified synthesis of IL-PLGA NPs. With the same PLGA and Acetonitrile as in the IL-PLGA synthesis, 5 mg/mL organic phase was added dropwise to a 3 mL aqueous phase of D_2O water with 20 mg of pre-dissolved PEG 8000 (Sigma Aldrich, #P2139-500G) and stirred at 1200 RPM and solvent evaporated for 3 hours at 25°C . Then, the EPP NPs were centrifuge-filtered with the 30 kDa filter tubes at 4°C and 2500 RPM for 50 mins. After bringing up to 3 mL with D_2O , 1 drop of IL was added to bare NPs at 800 RPM for 2 hours. Then the IL-EPP NPs were centrifuge-filtered at 2500 RPM for 50 mins at 4°C before being brought up to 1 mL total with D_2O and stored for up to 1 week at 4°C . The filtrate was brought up in 500 μL of D_2O and 0.2 mg of DSS was added for quantitative ^1H NMR spectroscopy and then to 1 mL for DLS measurements.

IL-DPP NP Synthesis: Using a modified version of the IL-PLGA synthesis, IL-DPP NPs were synthesized with 1 mg of the diblock copolymer PEG(5000)-b-PLGA(25000) (Sigma Aldrich, #799041-1G) in 101 μL of the Acetonitrile that was combined dropwise to a 10 mL aqueous phase of D_2O water at 1200 RPM. It was solvent evaporated at 25°C for 3 hours before the IL-DPP NPs were split into the 30 kDa filter tubes and centrifuged at 2500 RPM for 50 mins at 4°C . The NPs were recombined from splitting and brought up to 3 mL total in D_2O before 1 drop of IL was added at 800 RPM and left stirring for 2 hours. They were centrifuge-filtered again for 50 mins at 4°C before being resuspended in D_2O up to 1 mL and stored for 1 week at 4°C .

IL-EPP NP and IL-DPP NP Salt Titration: Bare EPP NPs were synthesized as explained above, and the filtrate was brought up in D_2O to a total of 3 mL of salt solution (0, 0.5 or 1.0 M of Na_2SO_4 salt). It spun for 2 mins before adding a drop of IL and left to spin for 2 hours. The same filtration as the coated EPP NPs was performed and the filtrate was resuspended in 500 μL of D_2O and quantitative ^1H NMR spectroscopy was performed with 0.2 mg of DSS. The NMR spectroscopy sample was then brought up to 1 mL and ran on DLS.

IL-EPP NP and IL-DPP NP Acid Titration After Salt: Bare and IL-NPs of the EPP and DPP NPs were synthesized and salt titrated as explained above. Once ^1H NMR spectroscopy and DLS characterization was performed, they were centrifuge-filtered at 2500 RPM for 15 minutes at 4°C to reconcentrate and filter out the DSS. The concentrated BARE and IL NPs were brought up to a final volume of 3 mL with the acidic D_2O phase and stirred for 2 minutes at 800 RPM (adding IL to the bare NPs) and room temperature. The filtration process was applied before running quantitative ^1H NMR spectroscopy and DLS measurements again on the acid titrated NPs.

IL-LDBC Synthesis: IL-LDBCs were synthesized as described by direct dissolution and nanoprecipitation as described previously¹³. Briefly, 1 mg of Polycaprolactone polyaminoamide amine (PCI-PAMAM 50: 50, NH_3^+ terminated, 50 kDa)⁴⁰ was combined with 50 μL neat IL/mg LDBC dropwise until submerging the polymer in a 20 mL glass scintillation vial at 25°C . The vial was then capped and sealed with parafilm and sonicated at 60°C until the LDBC was solvated by the neat IL. 2 mL of D_2O was added dropwise while vortexing the solution at the highest setting for 2 minutes, then sonicated at 25°C for 30 minutes. Finally, IL-LDBCs were centrifuge-filtered at 2500 RPM, 1 hour at 4°C in 4 mL Amicon 10 kDa filter tubes. Filtrates were resuspended to 1 mg/mL in D_2O buffer and stored at 4°C for up to 3 weeks.

IL-LDBC Salt Titration: The solvated phase of LDBC in neat IL (1 mg/50 μL) was formulated by direct dissolution as described above. Next, 2 mL of D_2O water consisting of 0 M, 0.5 M, or 1.0 M Na_2SO_4 was added dropwise while vortexing the solution at the highest setting for 2 minutes, then sonicated at 25°C for 30 minutes. Finally, IL-LDBCs were centrifuge-filtered at 2500 RPM, 1 hour at 4°C in 4 mL Amicon 10 kDa filter tubes (Millipore, #UFC801024). One mg filtrate was resuspended to 500 μL with D_2O for quantitative ^1H NMR spectroscopy with 0.2 mg DSS, which was then afterwards brought up to 1 mL for DLS measurements. Bare LDBCs were assembled as previously described^{13,40} and titrated by first combining 2 mg of PCI-PAMAM- NH_3^+ in 200 μL neat THF in a glass scintillation vial. This LDBC organic phase was vortexed for 2 minutes and sonicated briefly at 25°C to dissolve. While sonicating, 200 μL of LDBC organic phase was then added dropwise into a scint vial containing 2 mL of 0 M, 0.5 M, or 1.0 M Na_2SO_4 D_2O solution and continued to be sonicated for 2 hours at 25°C . Bare LDBCs were then parafilm-sealed and stored at 25°C overnight (ambient) to allow assembly. Afterwards, bare LDBCs were 10 kDa centrifuge-filtered at 2500 RPM for 50 minutes at 25°C and resuspended in D_2O to either 500 μL for ^1H NMR spectroscopy or DLS (1 mL) as specified above.

IL-LDBC Acid Titration After Salt: IL-LDBCs or bare LDBCs were formulated, salt-titrated, and characterized as described above. All LDBCs were then gently 10 kDa-filtered to re-concentrate at 2000 RPM for 30 minutes at either 25°C (bare LDBCs) or 4°C (IL-LDBCs). Using a glass Pasteur pipette, 2 mL D_2O at pH 4.8 (titrated with 0.25 M HCl in D_2O) was added dropwise to bare and IL-LDBC filtrates in a scintillation vial while vortexing the solution at the highest setting for 2 minutes, then sonicated at 25°C for 30 minutes. Finally, bare or IL-LDBCs were centrifuge-

filtered at 2500 RPM (at their respective temperatures), for 1 hour in 4 mL Amicon 10 kDa filter tubes. One milligram filtrate was then resuspended to 500 μ L with D₂O for quantitative ¹H NMR spectroscopy with 0.2 mg DSS, which was then afterwards brought up to 1 mL for DLS measurements. Due to the low intensity profile of PAMAM protons on ¹H NMR spectroscopy at 400 MHz, 2 mg (in 500 μ L) was used to study bare LDBC only, for which the calculations were then normalized to mol PAMAM/mg LDBC.

¹H NMR spectroscopy Calculations: A Bruker Ascend A300 (highest scan rate) or A400 (standard proton experiment) spectrometer was used to generate all proton NMR spectra. Mestre nova was used to analyze all spectra in triplicate (n = 3, standard deviation). During integration of IL and selected polymer peaks, DSS internal quantification standard was set to 9.00 and the ratio of protons to DSS was determined for signature singlet peaks (anion: CH₃, ~0.9 ppm; cation: 3(CH₃), ~3.2 ppm; PAMAM: ~1.6 ppm, PLGA: ~2.0 ppm) was calculated as a fraction (ex. 3H/12H), multiplied by the molarity of known DSS used (0.2 mg, MW: 224.36), and divided by the total mg of polymer material present. This generated total moles present in solution of anion or cation, respectively, which was summed and represented as moles IL/mg polymer. Total moles of IL/mg polymer was calculated by summing moles of anion and cation. A sample calculation is provided below, using the IL-PLGA system (0.5 M Na₂SO₄, replicate 1):

Part 1; Integration of identified peaks against DSS standard:

¹H NMR SPECTROSCOPY (400 MHz, D₂O) δ 6.66 (dt, J = 14.9, 6.9 Hz, 13H), 5.81 (d, J = 15.6 Hz, 14H), 4.74 (s, 449H), 4.06 (dq, J = 4.9, 2.8 Hz, 27H), 3.78 (td, J = 6.3, 3.2 Hz, 9H), 3.65 (dd, J = 11.6, 4.3 Hz, 21H), 3.59 – 3.49 (m, 46H), 3.20 (s, 128H), 2.23 – 2.12 (m, 28H), 2.08 (s, 31H), 1.45 (h, J = 7.4 Hz, 29H), 0.89 (t, J = 7.4 Hz, 44H), -0.00 (s, 9H).

Part 2; Calculation of IL component (mol) based on signature trans-2-hexenoate (2HA), choline, and polymer peaks:

$$\begin{aligned} \text{Anion: } & (44/9) * 8.91424496e-7 \text{ mol DSS} \\ & = 0.00000436 \text{ mol 2HA /mg PLGA} \\ \text{Cation: } & (128/9) * 8.91424496e-7 \text{ mol DSS} \\ & = 0.000012678 \text{ mol choline/mg PLGA} \\ \text{PLGA: } & (31/9) * 8.91424496e-7 \text{ mol DSS} \\ & = 0.00000307 \text{ mol PLGA /mg PLGA} \end{aligned}$$

Dynamic Light Scattering (DLS): Triplicate DLS measurements of all NPs after salt titration were conducted in a Zetasizer pro blue (Malvern, #MAL1252117). at the full 1 mL (1 mg NPs) in polystyrene cuvettes (DTS0012 cuvette, Sarstedt, #D-51588) to preserve the full content of polymer and IL material before acid titration. This ensured direct measurements were taken on the same samples that underwent acid treatment. For bare PLGA, bare LDBC, and their CA2HA-coated counterparts, zeta potential was measured using a palladium electrode dip cell (Malvern,

#ZEN1002). For all other systems, a disposable gold electrode zeta cell was used (Malvern, #DTS1070).

Separate controls were run during the methods optimization phase to ensure that running a concentrated sample produced equivalent results to the same samples traditionally further diluted for DLS (1: 10 v/v). After NMR spectroscopy post-acid titration, 1 mg/mL resuspended samples were then measured at a 1: 10 (v/v) dilution as some residual precipitation induced by the acid caused failed runs at the full undiluted 1 mL. While NP size is reported as its absolute value, zeta potentials are reported as the change in surface charge compared to non-treated bare or IL-coated NP controls. Averages with their standard deviation were calculated in triplicate (n = 3) in Microsoft Excel.

Acknowledgements

EELT acknowledges NSF Award #2204193, the support of the PhRMA Foundation, and the College of Liberal Arts at the University of Mississippi.

Conflict Of Interest

The authors have no conflicts of interest to declare.

References:

- (1) Correia, D. M.; Fernandes, L. C.; Fernandes, M. M.; Hermenegildo, B.; Meira, R. M.; Ribeiro, C.; Ribeiro, S.; Reguera, J.; Lanceros-Méndez, S. Ionic Liquid-Based Materials for Biomedical Applications. *Nanomaterials*. MDPI September 1, 2021. <https://doi.org/10.3390/nano11092401>.
- (2) Júlio, A.; Caparica, R.; Costa Lima, S. A.; Fernandes, A. S.; Rosado, C.; Prazeres, D. M. F.; Reis, S.; Santos de Almeida, T.; Fonte, P. Ionic Liquid-Polymer Nanoparticle Hybrid Systems as New Tools to Deliver Poorly Soluble Drugs. *Nanomaterials (Basel)* **2019**, *9* (8). <https://doi.org/10.3390/nano9081148>.
- (3) Fang, C.; Kong, L.; Ge, Q.; Zhang, W.; Zhou, X.; Zhang, L.; Wang, X. Antibacterial Activities of N-Alkyl Imidazolium-Based Poly(Ionic Liquid) Nanoparticles. *Polym Chem* **2019**, *10* (2), 209–218. <https://doi.org/10.1039/c8py01290c>.
- (4) Hamadani, C. M.; Goetz, M. J.; Mitragotri, S.; Tanner, E. E. L. *HEALTH AND MEDICINE Protein-Avoidant Ionic Liquid (PAIL)-Coated Nanoparticles to Increase Bloodstream Circulation and Drive Biodistribution*; 2020; Vol. 6. <https://www.science.org>.
- (5) He, Z.; Alexandridis, P. Ionic Liquid and Nanoparticle Hybrid Systems: Emerging Applications. *Advances in Colloid and Interface Science*. Elsevier B.V. June 1, 2017, pp 54–70. <https://doi.org/10.1016/j.cis.2016.08.004>.

- (6) Mishra, K.; Devi, N.; Siwal, S. S.; Zhang, Q.; Alsanie, W. F.; Scarpa, F.; Thakur, V. K. Ionic Liquid-Based Polymer Nanocomposites for Sensors, Energy, Biomedicine, and Environmental Applications: Roadmap to the Future. *Advanced Science*. John Wiley and Sons Inc September 1, 2022. <https://doi.org/10.1002/advs.202202187>.
- (7) Hayes, R.; Warr, G. G.; Atkin, R. Structure and Nanostructure in Ionic Liquids. *Chemical Reviews*. American Chemical Society July 8, 2015, pp 6357–6426. <https://doi.org/10.1021/cr500411q>.
- (8) McCrary, P. D.; Beasley, P. A.; Gurau, G.; Narita, A.; Barber, P. S.; Cojocaru, O. A.; Rogers, R. D. Drug Specific, Tuning of an Ionic Liquid's Hydrophilic-Lipophilic Balance to Improve Water Solubility of Poorly Soluble Active Pharmaceutical Ingredients. *New Journal of Chemistry* **2013**, 37 (7), 2196–2202. <https://doi.org/10.1039/c3nj00454f>.
- (9) Niemann, T.; Li, H.; Warr, G. G.; Ludwig, R.; Atkin, R. Influence of Hydrogen Bonding between Ions of like Charge on the Ionic Liquid Interfacial Structure at a Mica Surface. *Journal of Physical Chemistry Letters* **2019**, 10 (23), 7368–7373. <https://doi.org/10.1021/acs.jpcclett.9b03007>.
- (10) McDaniel, J. G.; Yethiraj, A. Understanding the Properties of Ionic Liquids: Electrostatics, Structure Factors, and Their Sum Rules. *Journal of Physical Chemistry B* **2019**, 123 (16), 3499–3512. <https://doi.org/10.1021/acs.jpccb.9b00963>.
- (11) Chen, J.; Dong, K.; Liu, L.; Zhang, X.; Zhang, S. Anti-Electrostatic Hydrogen Bonding between Anions of Ionic Liquids: A Density Functional Theory Study. *Physical Chemistry Chemical Physics* **2021**, 23 (12), 7426–7433. <https://doi.org/10.1039/d0cp06718k>.
- (12) Zhang, J.; Wang, W.; Zhang, Y.; Wei, Q.; Han, F.; Dong, S.; Liu, D.; Zhang, S. Small-Molecule Ionic Liquid-Based Adhesive with Strong Room-Temperature Adhesion Promoted by Electrostatic Interaction. *Nat Commun* **2022**, 13 (1). <https://doi.org/10.1038/s41467-022-32997-4>.
- (13) Hamadani, C. M.; Chandrasiri, I.; Yaddehige, M. L.; Dasanayake, G. S.; Owolabi, I.; Flynt, A.; Hossain, M.; Liberman, L.; Lodge, T. P.; Werfel, T. A.; Watkins, D. L.; Tanner, E. E. L. Improved Nanoformulation and Bio-Functionalization of Linear-Dendritic Block Copolymers with Biocompatible Ionic Liquids. *Nanoscale* **2022**, 14 (16), 6021–6036. <https://doi.org/10.1039/d2nr00538g>.
- (14) Chen, S.; Cheng, S. X.; Zhuo, R. X. Self-Assembly Strategy for the Preparation of Polymer-Based Nanoparticles for Drug and Gene Delivery. *Macromol Biosci* **2011**, 11 (5), 576–589. <https://doi.org/10.1002/mabi.201000427>.
- (15) Szutkowski, K.; Kołodziejska, Z.; Pietralik, Z.; Zhukov, I.; Skrzypczak, A.; Materna, K.; Kozak, M. Clear Distinction between CAC and CMC Revealed by High-Resolution NMR Diffusometry for a Series of Bis-Imidazolium Gemini Surfactants in Aqueous Solutions. *RSC Adv* **2018**, 8 (67), 38470–38482. <https://doi.org/10.1039/c8ra07081d>.
- (16) Astete, C. E.; Sabliov, C. M. *Synthesis and Characterization of PLGA Nanoparticles*; 2006; Vol. 17.

- (17) Fonseca, C.; Simoes, S.; Gaspar, R. *P Aclitaxel-Loaded PLGA Nanoparticles: Preparation, Physicochemical Characterization and in Vitro Anti-Tumoral Activity a a*; 2002; Vol. 83. www.elsevier.com/locate/jconrel.
- (18) Kocbek, P.; Obermajer, N.; Cegnar, M.; Kos, J.; Kristl, J. Targeting Cancer Cells Using PLGA Nanoparticles Surface Modified with Monoclonal Antibody. *Journal of Controlled Release* **2007**, *120* (1–2), 18–26. <https://doi.org/10.1016/j.jconrel.2007.03.012>.
- (19) Feczko, T.; Tóth, J.; Dósa, G.; Gyenis, J. Optimization of Protein Encapsulation in PLGA Nanoparticles. *Chemical Engineering and Processing: Process Intensification* **2011**, *50* (8), 757–765. <https://doi.org/10.1016/j.cep.2011.06.008>.
- (20) Bohrey, S.; Chourasiya, V.; Pandey, A. Polymeric Nanoparticles Containing Diazepam: Preparation, Optimization, Characterization, in-Vitro Drug Release and Release Kinetic Study. *Nano Converg* **2016**, *3* (1). <https://doi.org/10.1186/s40580-016-0061-2>.
- (21) Yadav, K. S.; Sawant, K. K. Modified Nanoprecipitation Method for Preparation of Cytarabine-Loaded PLGA Nanoparticles. *AAPS PharmSciTech* **2010**, *11* (3), 1456–1465. <https://doi.org/10.1208/s12249-010-9519-4>.
- (22) Kelly, J. M.; Gross, A. L.; Martin, D. R.; Byrne, M. E. Polyethylene Glycol-b-Poly(Lactic Acid) Polymersomes as Vehicles for Enzyme Replacement Therapy. *Nanomedicine* **2017**, *12* (23), 2591–2606. <https://doi.org/10.2217/nnm-2017-0221>.
- (23) Locatelli, E.; Franchini, M. C. Biodegradable PLGA-b-PEG Polymeric Nanoparticles: Synthesis, Properties, and Nanomedical Applications as Drug Delivery System. *Journal of Nanoparticle Research*. Kluwer Academic Publishers December 1, 2012. <https://doi.org/10.1007/s11051-012-1316-4>.
- (24) Zhang, X.; Zhang, P. Polymersomes in Nanomedicine - A Review. *Curr Nanosci* **2017**, *13* (2), 124–129. <https://doi.org/10.2174/1573413712666161018144519>.
- (25) Wurm, F.; Frey, H. Linear-Dendritic Block Copolymers: The State of the Art and Exciting Perspectives. *Progress in Polymer Science (Oxford)*. January 2011, pp 1–52. <https://doi.org/10.1016/j.progpolymsci.2010.07.009>.
- (26) Zhang, K.; Tang, X.; Zhang, J.; Lu, W.; Lin, X.; Zhang, Y.; Tian, B.; Yang, H.; He, H. PEG-PLGA Copolymers: Their Structure and Structure-Influenced Drug Delivery Applications. *Journal of Controlled Release*. Elsevier June 10, 2014, pp 77–86. <https://doi.org/10.1016/j.jconrel.2014.03.026>.
- (27) Winterton, N. Solubilization of Polymers by Ionic Liquids. *J Mater Chem* **2006**, *16* (44), 4281–4293. <https://doi.org/10.1039/b610143g>.
- (28) Liu, S.; Walton, M.; Tarakina, N. V.; Akcora, P. Solvation in Ionic Liquids with Polymer-Grafted Nanoparticles. *Journal of Physical Chemistry B* **2020**, *124* (23), 4843–4850. <https://doi.org/10.1021/acs.jpcc.0c02813>.
- (29) Zhou, Y.; Bie, C.; van Zijl, P. C. M.; Xu, J.; Zou, C.; Yadav, N. N. Detection of Electrostatic Molecular Binding Using the Water Proton Signal. *Magn Reson Med* **2022**, *88* (2), 901–915. <https://doi.org/10.1002/mrm.29230>.

- (30) Meltzer, R. H.; Thompson, E.; Soman, K. V.; Song, X.-Z.; Ebalunode, J. O.; Wensel, T. G.; Briggs, J. M.; Pedersen, S. E. Electrostatic Steering at Acetylcholine Binding Sites. *Biophys J* **2006**, *91* (4), 1302–1314. <https://doi.org/10.1529/biophysj.106.081463>.
- (31) Meier, D. M.; Urakawa, A.; Turrà, N.; Rügger, H.; Baiker, A. Hydrogen-Bonding Interactions in Cinchonidine-2-Methyl-2-Hexenoic Acid Complexes: A Combined Spectroscopic and Theoretical Study. *J Phys Chem A* **2008**, *112* (27), 6150–6158. <https://doi.org/10.1021/jp801866p>.
- (32) Karlsson, E.; Shin, J. H.; Westman, G.; Eriksson, L. A.; Olsson, L.; Mapelli, V. In Silico and in Vitro Studies of the Reduction of Unsaturated α,β Bonds of Trans-2-Hexenedioic Acid and 6-Amino-Trans-2-Hexenoic Acid – Important Steps towards Biobased Production of Adipic Acid. *PLoS One* **2018**, *13* (2). <https://doi.org/10.1371/journal.pone.0193503>.
- (33) Saha, D.; Kumar, S.; Ray, D.; Mata, J.; Aswal, V. K. Structure and Stability of Biodegradable Polymer Nanoparticles in Electrolyte Solution. *Materials Letters: X* **2021**, *10*. <https://doi.org/10.1016/j.mlblux.2021.100066>.
- (34) Inam, W.; Bhadane, R.; Akpolat, R. N.; Taiseer, R. A.; Filippov, S. K.; Salo-Ahen, O. M. H.; Rosenholm, J. M.; Zhang, H. Interactions between Polymeric Nanoparticles and Different Buffers as Investigated by Zeta Potential Measurements and Molecular Dynamics Simulations. *VIEW* **2022**, *3* (4). <https://doi.org/10.1002/VIW.20210009>.
- (35) Kim, Y. G.; Thérien-Aubin, H. Impact of the Solvent Quality on the Local Dynamics of Soft and Swollen Polymer Nanoparticles Functionalized with Polymer Chains. *Macromolecules* **2020**, *53* (17), 7561–7569. <https://doi.org/10.1021/acs.macromol.0c00346>.
- (36) Liu, S.; Liedel, C.; Tarakina, N. V.; Osti, N. C.; Akcora, P. Dynamics of Ionic Liquids in the Presence of Polymer-Grafted Nanoparticles. *Nanoscale* **2019**, *11* (42), 19832–19841. <https://doi.org/10.1039/c9nr04204k>.
- (37) Suen, J. W.; Elumalai, N. K.; Debnath, S.; Mubarak, N. M.; Lim, C. I.; Reddy, M. M. The Role of Interfaces in Ionic Liquid-Based Hybrid Materials (Ionogels) for Sensing and Energy Applications. *Advanced Materials Interfaces*. John Wiley and Sons Inc December 2, 2022. <https://doi.org/10.1002/admi.202201405>.
- (38) Saielli, G.; Wang, Y. Role of the Electrostatic Interactions in the Stabilization of Ionic Liquid Crystals: Insights from Coarse-Grained MD Simulations of an Imidazolium Model. *J Phys Chem B* **2016**, *120* (34), 9152–9160. <https://doi.org/10.1021/acs.jpcc.6b04717>.
- (39) Parkins, A. W.; Prince, P. D.; Smith, R. A.; Steed, J. W. Chromous Hydrazine Sulfate. *Acta Crystallogr C* **2001**, *57* (Pt 6), 670–671. <https://doi.org/10.1107/s0108270101000919>.
- (40) Chandrasiri, I.; Abebe, D. G.; Loku Yaddehige, M.; Williams, J. S. D.; Zia, M. F.; Dorris, A.; Barker, A.; Simms, B. L.; Parker, A.; Vinjamuri, B. P.; Le, N.; Gayton, J. N.; Chougule, M. B.; Hammer, N. I.; Flynt, A.; Delcamp, J. H.; Watkins, D. L. Self-Assembling PCL-PAMAM Linear Dendritic Block Copolymers (LDBC)s for Bioimaging and Phototherapeutic Applications. *ACS Appl Bio Mater* **2020**, *3* (9), 5664–5677. <https://doi.org/10.1021/acsabm.0c00432>.

